Available online at www.sciencedirect.com

ScienceDirect

Ceramics International 40 (2014) 1641–1649

CERAMICS INTERNATIONAL

www.elsevier.com/locate/ceramint

The influence of disorder on the appearance of Griffiths phase and magnetoresistive properties in $(La_{1-x}Nd_x)_{2/3}(Ca_{1-y}Sr_y)_{1/3}MnO_3$ oxides

J. Khelifi[a,b,*], A. Tozri[a], F. Issaoui[a], E. Dhahri[a], E.K. Hlil[b]

[a]*Laboratoire de Physique Appliquée, Faculté des Sciences, B.P. 1171, 3000 Sfax, Université de Sfax, Tunisie*
[b]*Institut Néel, CNRS et Université Joseph Fourier, BP 166, F-38042 Grenoble Cedex 9, France*

Received 12 April 2013; received in revised form 4 June 2013; accepted 10 July 2013
Available online 18 July 2013

Abstract

The effect of quenched disorder on the magnetic and transport properties of $(La_{1-x}Nd_x)_{2/3}(Ca_{1-y}Sr_y)_{1/3}MnO_3$ polycrystalline samples with (***J1***($x=0$, $y=0$); ***J2***($x=0.05$,$y=0.04$); ***J3*** ($x=0.25$,$y=0.20$); ***J4***($x=0.3$,$y=0.24$); ***J5***($x=0.98$,$y=0.8$) is analyzed within the context of percolative transport and the existence of the Griffiths phase. Our results demonstrate that moderate-small chemical disorder affects the inverse dc susceptibility χ^{-1}(T) at higher temperature revealing the presence of the Griffiths phase above the Curie temperature. We attribute the observed anomalous paramagnetic behavior to the magnetic heterogeneity caused by the segregation of short-range ferromagnetic clusters within the paramagnetic matrix. The electrical properties show the presence of a metal-insulator transition at T_{MI} which decreases with increasing disorder σ^2. In the low-temperature ferromagnetic metallic region, the ρ data follow an empirical relation, $\rho_{FM}=\rho_0+\rho_2T^2+\rho_{4.5}T^{4.5}$ reflecting that the conductive mechanism mainly arises from electron–electron, electron–phonon and electron–magnon scattering changed versus disorder effect. In the high-temperature paramagnetic insulating region, the ρ data for all samples follow the adiabatic small-polaron-hopping model. To understand the dependence of disorder with transport mechanism, we used the phenomenological equation for conductivity under a percolation approach, which is dependent on the phase segregation of ferromagnetic metallic clusters and paramagnetic insulating regions. Also we demonstrate that magnetoresistance (MR) increase with increasing disorder σ^2. It is very interesting to note that the MR at room temperature is enhanced, which is encouraging for potential applications.

Keywords: Griffiths phase; Manganites; Magnetoresistance; Percolation; Quenched disorder

1. Introduction

In recent years, the manganites with $R_{1-x}B_xMnO_3$ formula (R=rare-earth cation, B=alkaline-earth cation) have been extensively studied because of their richness in physical properties which is due to the simultaneous presence of spin, lattice and orbital degrees of freedom [1,2]. Significant attention has been paid by researchers in order to explore their potential for wide range of technological applications such as read heads, magnetic information storage, magnetocaloric effect (MCE), magnetoresistance properties (*CMR*) and more recently spintronic applications [3–5]. Many factors affect the magnetic and the transport properties such as, the average ionic radius of the A-site ($\langle r_A \rangle$), the doping concentration x which determine the Mn^{3+}/Mn^{4+} ratio, the magnetic moment of the rare earth ions present at the A-site that may couple to the Mn ions and the cation size mismatch (σ^2). The *CMR* behavior, is usually explained with double exchange (*DE*) theory based on the exchange of electrons between Mn^{3+} and Mn^{4+} ions [6], additional effects, e.g. the strong Jahn–Teller (JT) interactions, phase separation are reported to play important roles in these materials [7,8] and is due also to the existence of quenched disorder which induces nanoscale spin clusters in the paramagnetic region [9,10]. This feature leads to the Griffiths phase (GP) [11] which originally proposed for randomly diluted Ising ferromagnet where only a fraction of the lattice sides are occupied with spins and rest are either vacant or filled with nonmagnetic atoms without spins. The GP means the existence of short range ferromagnetic

*Corresponding author at: Laboratoire de Physique Appliquée, Faculté des Sciences, B.P. 1171, 3000 Sfax, Université de Sfax, Tunisie.
Tel.: +216 22 262936.
E-mail address: klifijaber@yahoo.fr (J. Khelifi).

0272-8842/$ - see front matter © 2013 Elsevier Ltd and Techna Group S.r.l. All rights reserved.
http://dx.doi.org/10.1016/j.ceramint.2013.07.055

(FM) clusters in paramagnetic matrix in the temperature range $T_C \leq T \leq T_G$ (T_G generally called Griffiths temperature), in this region, such a system exhibits a sharp downturn in the high temperature inverse susceptibility (χ^{-1}) and can be recognized as a typical manifestation of GP [11,12].

Here, we present a survey of the effect of the random distribution of the A-site cations on the magnetic and transport properties. We have chosen the series of compounds $(La_{1-x}Nd_x)_{2/3}(Ca_{1-y}Sr_y)_{1/3}MnO_3$, by appropriate substitutions, simultaneously of La by Nd and Ca by Sr, both the fraction Mn^{3+}/Mn^{4+} and the average ionic radius of the A-site $\langle r_A \rangle$ has been maintained constant but different values of variance σ^2 ranging from 0.5287 10^{-3} to 4.3247 10^{-3} Å^2.

2. Materials and methods

A series of samples $(La_{1-x}Nd_x)_{2/3}(Ca_{1-y}Sr_y)_{1/3}MnO_3$ with the same *A*-site cational mean radius $\langle r_A \rangle$ =1.2038 Å and the same average valence of the Mn ion (3.33) but different *A* site ionic radii variance σ^2 (defined as $\sigma^2 = \sum y_i r_i^2 - (\sum y_i r_i)^2 = \langle r_A^2 \rangle - \langle r_A \rangle^2$) were chosen for the present study. All the ceramics samples were prepared by the conventional solid-state reaction in air was described in previous work [13]. The resistivity measurement without and with magnetic field (0,1,3, and 5 T) are carried out using four-probe method in the temperature range from 2 to 400 K on a quantum design Physical Property Measurement System (PPMS Model). Magnetic measurements were realized with the *BS2* magnetometer developed at Néel Institute. This magnetometer uses extraction technique and can produce a field of 10 T.

3. Results and discussions

3.1. Magnetic study

The temperature dependence of magnetization M(T) for all samples $(La_{1-x}Nd_x)_{2/3}(Ca_{1-y}Sr_y)_{1/3}MnO_3$ was investigated in previous work [13]. With increasing σ^2 there is no change in nature of the magnetic transition which remains PM-FM without any anomalies detected at low temperature. However, the increase of σ^2 causes a decrease in the magnetization and shift T_C to the low temperature. The transition temperature T_C decreases with increasing disorder σ^2 from 255 K to 230 K see Table 1.

Fig. 1 shows the inverse dc susceptibility χ^{-1}(T) (defined as $M/H)^{-1}$ as a function of the temperature for the five $(La_{1-x}Nd_x)_{2/3}(Ca_{1-y}Sr_y)_{1/3}MnO_3$ samples with different values of disorder σ^2 under different applied field H. (***J1***) 0.05287×10^{-3}; (***J2***) 0.06418×10^{-3}; (***J3***) 1.335×10^{-3}; (***J4***) 1.4481×10^{-3}; (***J5***) 4.3247×10^{-3}. It is well known that in the paramagnetic (PM) region, the relation between χ and the temperature T should follow the Curie–Weiss law (CW), i.e.$\chi = C/(T-\theta P)$, where C is the Curie constant and θ_P is the Weiss temperature. The linear fit in Fig. 1 is the fitting curves deduced from the Curie–Weiss equation. The best-fit parameters are summarized in Table 1 together with the theoretically paramagnetic effective moments which were calculated from the Curie constant using the above equation (i.e. calculated for free Mn^{3+} ($S=2$) and Mn^{4+} ($S=3/2$), ($\mu_{eff} = g\sqrt{S(S+1)}$) considering a spin-only contribution and Nd^{3+} ($J=9/2$) considering a spin-orbit contribution) $\mu_{eff} = g\sqrt{J(J+1)}$, where "g" is the Landé factor, "S" is the spin of the cation and μ_B is the Bohr magneton and $J = L \pm S$. The values of μ_{eff}^{the} and μ_{eff}^{exp} grouped in Table 1 indicate that the experimental effective moments μ_{eff}^{exp} calculated from fitting to the Curie–Weiss law are significantly larger than the expected theoretically values (Mn+Nd). Indeed, this difference is probably due to a disorder introduced by size mismatch effect and also due to a FM correlation in the paramagnetic state that is likely attributable to FM cluster formations (FM polarons). The existence of short-range FM interactions well above T_C was proposed for $La_{0.67}Ca_{0.33}MnO_3$ where magnetic clusters were detected from small angle neutron scattering by De Teresa et al. [14]. This kind of magnetic cluster in the PM

Table 1
Magnetic data for all specimens of $(La_{1-x}Nd_x)_{2/3}(Ca_{1-y}Sr_y)_{1/3}MnO_3$. The experimental effective paramagnetic moment μ_{eff}^{exp}, the theoretical effective paramagnetic momentμ_{eff}^{the}, *C* is the Curie constant and θ_P is the temperature paramagnétique. The parameters evaluated from Griffiths model: T_C^{Rand} is the disorder dependent FM ordering temperature, T_G is the Griffiths temperature and λ is the exponent characterizing strength of Griffiths phase and GP (%) the temperature range of GP and T_f is the temperature derivative of the volume fraction *f*.

Samples	***J1***	***J2***	***J3***	***J4***	***J5***
Compositions	$x=0$, $y=0$	$x=0.05$, $y=0.04$	$x=0.25$, $y=0.20$	$x=0.3$, $y=0.24$	$x=0.98$, $y=0.8$
$\sigma^2 \times 10^{-3}$ (Å^2)	0.5284	0.6418	1.335	1.4481	4.3247
C(*K*.uem/mol)	5.891	5.545	4.622	5.177	5.891
θ_P (*K*)	236.223	242.725	253.198	244.282	205.367
μ_{eff}^{exp} (μ_B)	6.865	6.661	6.081	6.435	5.891
μ_{eff}^{the} (μ_B)	4.582	4.629	4.814	4.861	5.437
T_C	255	250	245	240	230
T_{MI}	265	265	250	250	245
T_G (K)	261	261	258	276	256
T_f (K)	260	260	245	260	255
T_C^{Rand} (K)	252	250	251	250	230
λ	0.381 ± 0.01	0.311 ± 0.028	0.133 ± 0.01	0.326 ± 0.023	0.356 ± 0.011
GP (%)	2.35	4.4	5.306	15	11.304

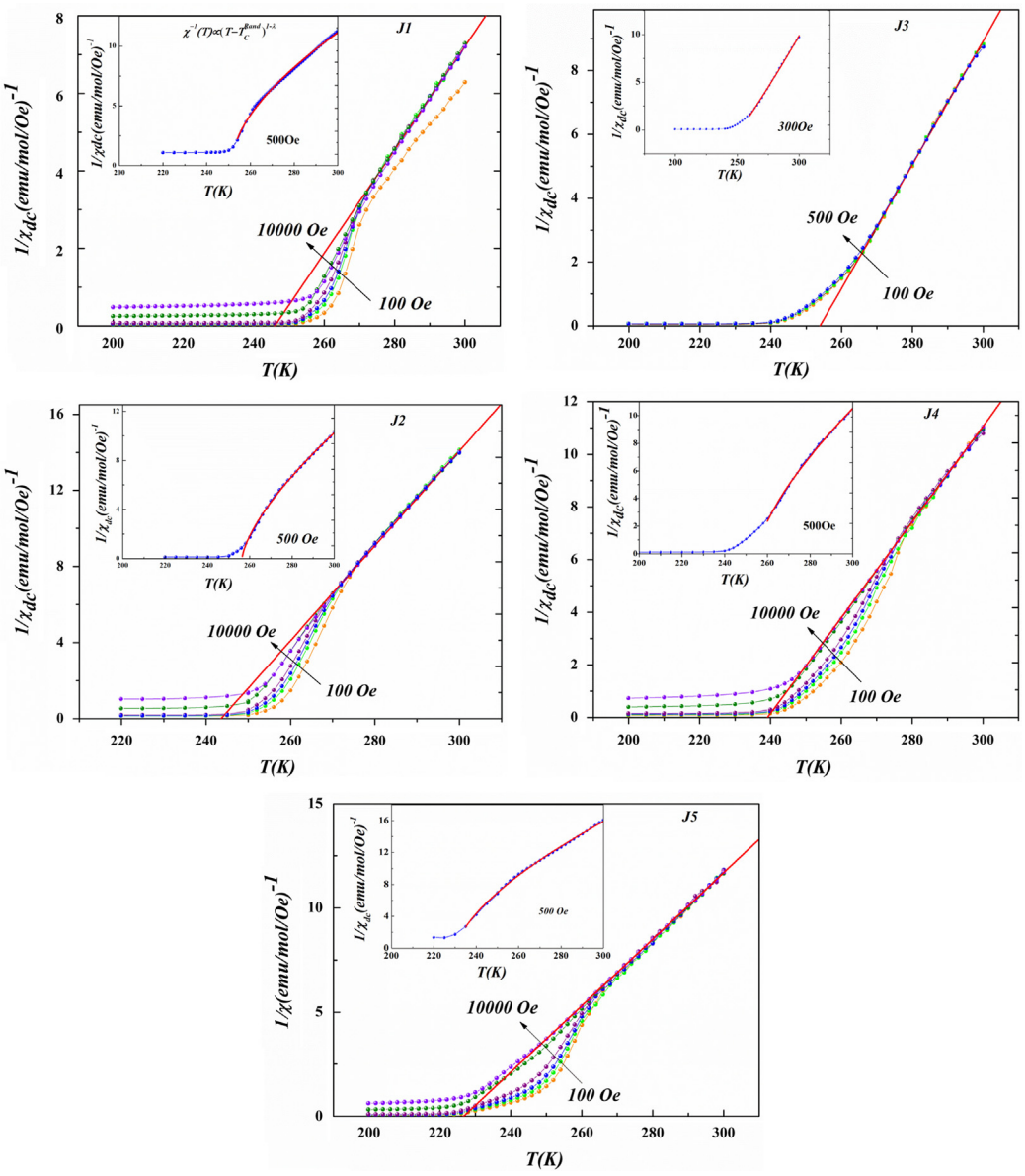

Fig. 1. Temperature dependence of the inverse magnetic susceptibility for a series of $(La_{1-x}Nd_x)_{2/3}(Ca_{1-y}Sr_y)_{1/3}MnO_3$ samples with variance σ^2: (***J1***) 0. 05287×10^{-3}; (***J2***) 0. 06418×10^{-3}; (***J3***) 1.335×10^{-3}; (***J4***) 1.4481×10^{-3}; (***J5***) 4.3247×10^{-3}at various magnetic fields (H=0.01, 0.03, 0.05, 0.1, 0.5 and 1 T). Straight lines show the Curie–Weiss law fitting of susceptibility data above T_C. The inset shows the inverse dc susceptibility obtained from magnetization measurements in a field of 500 Oe for sample J1, J2, J4, J5 and 300 Oe for sample J3. The solid lines are the fits with the power law equation:$\chi^{-1}(T)\propto(T-T_C^{Rand})^{1-\lambda}$

region have been shown for single crystal $Pr_{0.50+x}Sr_{0.50-x}MnO_3$ [15] and other manganites in both single crystal [16] as well as in polycrystalline samples [17] and are thought to be an intrinsic property of manganites. In the classic work of Imry and Ma [18], it was supposed that random quenched disorder arising from lattice defects or chemical substitution can destabilize the long-range order system favoring formation of 'finite-size' clusters and appearance of coexisting clusters and their size regulation by disorder in manganites has also been shown from simulation work by Moreo et al. [19].

The presence of clusters FM in the PM phase in $(La_{1-x}Nd_x)_{2/3}(Ca_{1-y}Sr_y)_{1/3}MnO_3$ samples may be due to the signature of Griffiths-like phase or polarons magnetic in the paramagnetic phase.

Many models were suggested to solve the problem of magnetic susceptibility in manganites (i.e. the deviation from the Curie–Weiss law). One of them has been proposed by Yi et al. [20], who performed Monte Carlo calculations on a single-orbital DE Hamiltonian and interpreted the resulting PM susceptibility in terms of spin clusters and the formation of magnetic polarons. The other one indicated the presence of GP in dilute ferromagnets [11], which was used by Salamon and Chun [9] to analyze their susceptibility and heat capacity data on $La_{0.7}$ (Ba, Ca, Sr)$_{0.3}$ MnO_3 near T_C.

In order to verify the existence of Griffiths-like phase in all samples in the form of FM cluster system within a PM matrix, macroscopic magnetization experiments were carried out by [11,21]. From the (inset Fig. 1), the χ^{-1} (T) shows a clear

downturn at temperature above T_C. These pictures illustrate clearly the anomalous behavior of $\chi^{-1}(T)$ that represents the fingerprint of GP.

To demonstrate the evolution of the GP according to external field, we measured additionally the inverse dc magnetic susceptibility $\chi^{-1}(T)$ curves by varying field ($H=0.01$, 0.03, 0.05, 0.1, 0.5, and 1 T) in the high-temperature range ($200 \leq T \leq 300$ K) for all the doped samples, as shown in Fig. 1. We note that GP is suppressed at high field for ***J1***, ***J2***, ***J4*** and ***J5*** samples under field 1 T. In contrast, the samples ***J3*** presents a GP which disappears at field of 500 Oe. The $\chi^{-1}(T)$ fully obeys the conventional Curie–Weiss law in the PM state. Based on the original paper of Griffiths [11], and subsequent work [9,21], this suppression is another characteristic of GP and this is due to polarization of spins outside the clusters or in terms of the masking of the FM signal by the rising PM background, as already proposed by Salamon et al., [9] in manganite systems. It has been shown that the GP is univocally characterized by a magnetic susceptibility exponent lower than unity [21,22], i.e., characterized by a power law [11].

$$\chi^{-1}(T) \propto (T - T_C^{Rand})^{1-\lambda} \quad (1)$$

where $(0 < \lambda < 1)$ is the exponent characterizing strength of "Griffiths phase" and T_C^{Rand} is the critical temperature of the random ferromagnet. The choice of T_C^{Rand} has been less precise. Here, for determining T_C^{Rand} one uses the method already used and described by Jiang et al. [21]. The associated accuracy in the estimate for T_C^{Rand} using this criterion is 1 K. To calculate λ, we have fitted Eq. (1). This power-law relation appears to be a modified form of CW law where the exponent λ signifies deviation from the CW behavior. In the pure paramagnetic region, λ is expected to be zero. The GP is characterized by the presence of "finite-size" FM clusters within PM matrix above T_C. In addition another study show the presence of the GP by the magnetization follows [23]:

$$M(H,T) \alpha \exp(-C(T/H)) \quad (2)$$

where C is a constant (proportional to the total moment of magnetic cluster).This formula is employed to fit the $M(T)$ curves which not only confirms the existence of GP but also indicates the important role of disorder in the formation of GP.

Table 1 shows clearly the variation of λ signature of GP. We note the existence of GP for ***J1***, ***J2***, ***J4*** and ***J5*** samples. The magnetization of the sample ***J3*** have a downturn in the χ^{-1}(T) vs. T curve at low fields $H=100$ and 300 Oe which suppressed at $H=500$ Oe and the estimated value of T_G is 258 K. the corresponding exponent λ obtained from the power low Eq. (1) is very close to $\lambda=0.133$ which confirm the presence of GP which disappear at low field 500 Oe ($\lambda=0.03125$).

However it is clear from Table 1 that the temperature range of GP normalized with the respective T_Cs calculated as GP (%GP)$=[(T_G-T_C)/T_C] \times 100$ increases with quenched disorder. In addition, the Griffiths transition temperatures T_G value change in different optimally-doped $(La_{1-x}Nd_x)_{2/3}(Ca_{1-y}Sr_y)_{1/3}MnO_3$ samples.

In order to investigate the influence of the quenched disorder, induced by the random substitution of La^{+3} by ions with different sizes and valences, we can see the variation of the Griffiths exponent λ and the difference between T_G and T_C^{Rand}. The variation of λ in $(La_{1-x}Nd_x)_{2/3}(Ca_{1-y}Sr_y)_{1/3}MnO_3$ samples ***J1***, ***J2***, ***J4*** and ***J5*** is related to the size of ferromagnetic clusters. For J3 the contribution of FM clusters to the total magnetic susceptibility of the system is dominated by that of PM cluster. The lower difference between T_G and T_C^{Rand} indicates that GP is reduced. It is seen that when the A-site disorder increases, the number of clusters and GP extends to a greater temperature range [22]. Hence, the observations of the Griffiths singularity in our systems highlight the presence of a correlated quenched disorder. However, introducing quenched disorder in manganite in the form of chemical substitutions remains a challenging task, as the introduction of dissimilar ion (s) at site A leading to a change in structure, which modifies the original system completely (in our system no change in structure of $(La_{1-x}Nd_x)_{2/3}(Ca_{1-y}Sr_y)_{1/3}MnO_3$) [13]. Whereas, the introduction of magnetic elements in $(La_{1-x}Nd_x)_{2/3}(Ca_{1-y}Sr_y)_{1/3}MnO_3$ will modify the basic system by introducing additional magnetic interactions. It is not the same interactions between magnetic elements in all samples Mn–O–Mn; Nd–O–Mn and Nd–O–Nd. However, the Nd ionic doping interrupts the connection of long-range Mn chains and introduces the magnetic disorder into the system. The chemical disorder induces magnetic inhomogeneity that along with charge, spin, and lattice degrees of freedom, has a notable impact on the magnetic ordering in doped manganites, in particular in low-hole-doped [24] and half-doped [25] compounds. It seems that mesoscale chemical disorder may be responsible for appearance of small FM polarons in the PM state of sample ***J3*** with $\sigma^2=1.335 \times 10^{-3}$ Å^2 or such clusters seem to be absent or having very low concentration of clusters FM in this sample and also the existence of FM-like correlations in the PM state associated with the appearance of spin clusters having nonzero net magnetic moments.

3.2. Electrical measurements

Fig. 2 shows the variation of temperature dependence of resistivity for $(La_{1-x}Nd_x)_{2/3}(Ca_{1-y}Sr_y)_{1/3}MnO_3$ samples with disorder σ^2 under zero magnetic applied field. All samples are found to exhibit a transition from high- temperature insulating behaviors (i.e $d\rho/dT < 0$) to low- temperature metallic behaviors at (i.e $d\rho/dT > 0$) according with other systems previously studied [26,27]. We can see that the metal–insulator transition temperature (T_{MI}) decreases slightly with the increase of disorder σ^2 from 265 K to 245 K (see Table 1). The decrease of T_{MI} with the *A*-site mismatch σ^2 is due to the substitutions of La^{3+} by Nd^{3+} and Ca^{2+} by Sr^{2+} ions that decreases the tendencies of charge localization due to the enhancement in the mobility of hopping electrons, which suppress metallicity and push the system in the insulator side. With increasing disorder σ^2 there is no change in nature of the electrical transition which remains *M–I* without any anomalies detected at low and high temperature such as charge ordered.

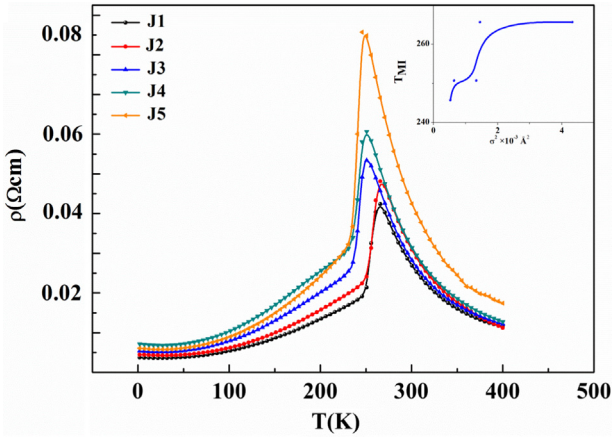

Fig. 2. Variation of resistivity with temperature of $(La_{1-x}Nd_x)_{2/3}(Ca_{1-y}Sr_y)_{1/3}MnO_3$ under zero magnetic applied field.

Another peculiarity can be explored related to the influence of the *A*-site disorder on the maximum of resistivity which increases slightly from 0.0424 Ωcm to 0.0857 Ωcm for $(La_{1-x}Nd_x)_{2/3}(Ca_{1-y}Sr_y)_{1/3}MnO_3$ samples and localizes the charge carriers. We show slightly an increase on the maximum of resistivity and a decrease of the metal– insulator transition temperature (T_{MI}) in all samples.

For the description of the transport properties of $(La_{1-x}Nd_x)_{2/3}(Ca_{1-y}Sr_y)_{1/3}MnO_3$ manganite, we suppose a percolation character of the metal–insulator transition. To show the mixed-phase percolative conduction from the phenomenological view, the standard percolation scenario obtained from the simulation is illustrated in Fig. 3 for the transition from the FMM phase to PMI phase with the increased *T*.

Fig. 3 shows the evolution of the resistivity in the temperature intervals 200 K–400 K under different magnetic applied fields up to 5 T for $(La_{1-x}Nd_x)_{2/3}(Ca_{1-y}Sr_y)_{1/3}MnO_3$ samples fitted by the model of Li et al. [28] based on the phase segregation mechanism. The solid line in Fig. 3 presents the fitting results for the ρ (*T*) curves. This model is clearly elucidates the transport mechanism in the whole measured temperature region of manganites. Therefore, in order to explain the origin of the low temperature resistivity, the experimental data have been analyzed using the following empirical equation:

$$\rho_{FM}(T) = \rho_0 + \rho_2 T^2 + \rho_{4.5} T^{4.5} \quad (3)$$

where ρ_0 is the residual resistivity arises due to grain or domain boundaries. The ρ_2 term represents the electrical resistivity due to the electron–electron scattering process and is generally dominant up to 100 K [29].On the other hand, the term $\rho_{4.5}$ is a combination of electron–electron, electron–magnon and electron–phonon scattering processes [30].

While for the high temperature (above the T_{MI}) the dependence of ρ (*T*) is well analyzed by the thermo activated law given by

$$\rho_{PM}(T) = \rho_\alpha \exp\left(\frac{E_a}{K_B T}\right) \quad (4)$$

where E_a is the activation energy and ρ_α is the coefficient independent from *T* and K_B is the Boltzmann constant. The

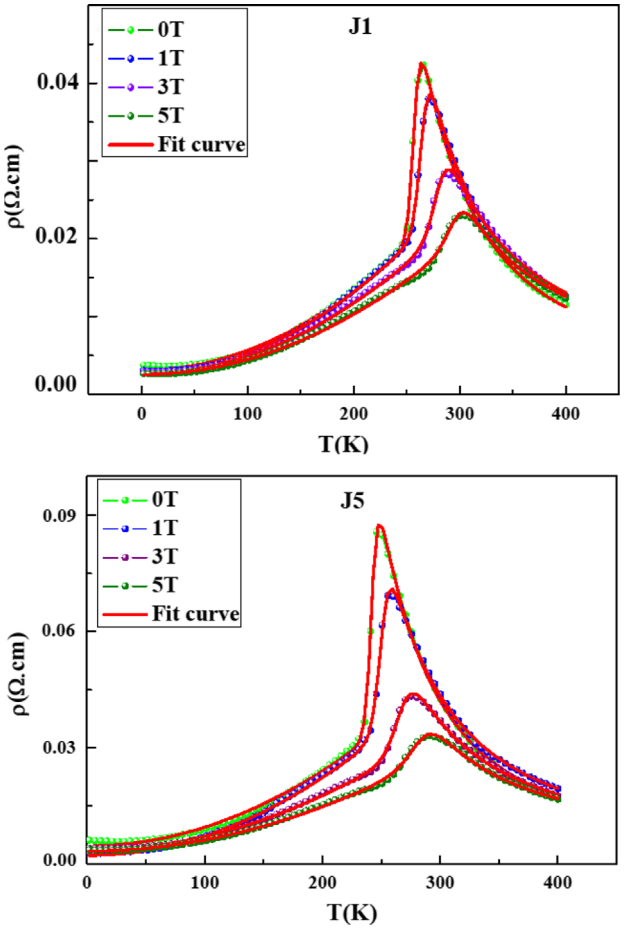

Fig. 3. Electrical resistivity (ρ) as a function of temperature (*T*) of $(La_{1-x}Nd_x)_{2/3}(Ca_{1-y}Sr_y)_{1/3}$ MnO_3 samples under applied magnetic field of 0, 1, 3 and 5 T. The solid lines are the fits with the equation $\rho(T) = f \times (\rho_0 + \rho_2 T^2 + \rho_{4.5} T^{4.5}) + (1-f) \times \rho_\alpha \exp(\frac{E_a}{K_B T})$.

values of approximation coefficients (ρ_0, ρ_2, $\rho_{4.5}$, ρ_α, and E_a) included in formulas (3) and (4) are described in works [30,31]. As mentioned above, considering the percolation character of the metal–insulator transition, the total resistivity can be expressed as

$$\rho(T) = f \times \rho_{FM} + (1-f) \times \rho_{PM} \quad (5)$$

where *f* and $(1-f)$ are the volume concentrations of the ferromagnetic and the paramagnetic phases, respectively. The volume concentrations of the two phases satisfy the Boltzman distribution

$$f = \frac{1}{1+\exp(\Delta u / K_B T)} \quad (6)$$

where $\Delta U = U_0(1-(T/T_C^{\mathrm{mod}}))$ is the difference in energy between the ferromagnetic FMM and the paramagnetic PMI state, T_C^{mod} is a PMI-FMM transition temperature used in the model and near/equal to T_C. Hence the complete expression describing the resistivity dependence as a function of temperature will take the form

$$\rho(T) = f \times (\rho_0 + \rho_2 T^2 + \rho_{4.5} T^{4.5}) + (1-f) \times \rho_\alpha \exp\left(\frac{E_a}{K_B T}\right) \quad (7)$$

The results obtained by the approximation of the experimental data using expressions (6),(7) are presented in Table 2. The values

Table 2
Obtained parameters corresponding to the best fit to the Eq. (6) of the experimental data of $(La_{1-x}Nd_x)_{2/3}(Ca_{1-y}Sr_y)_{1/3}MnO_3$ samples (***J1***) 0. 05287 × 10^{-3}; (***J2***) 0. 06418 × 10^{-3}; (***J3***) 1.335 × 10^{-3}; (***J4***) 1.4481 × 10^{-3}; (***J5***) 4.3247 × 10^{-3} at 0, and 5 T.

H(T)	ρ_0 (Ωcm)	ρ_2(Ωcm/K^2)	$\rho_{4.5}$(Ωcm/K$^{4.5}$)	ρ_α(Ωcm)	E_a/K_B (K)	ΔU/K_B (K)	T_C^{mod} (K)
J1 (x=0, y=0)							
0 T	0.00153	2.556E−7	3.129E−4	8.392E−7	1402.794	22721.399	257
5 T	0.00152	1.933E−7	2.031E−4	1.593E−6	1193.327	13045.999	297
J2(x=0.05, y=0.04)							
0 T	0.00157	3.007E−7	3.946E−4	6.753E−7	1522.275	21768.124	259
5 T	6.218E−4	1.751E−7	3.244E−4	9.991E−7	1275.103	13475.098	291
J3(x=0.25, y=0.20)							
0 T	0.00223	3.852E−7	4.439E-4	9.543E−7	1378.599	19301.726	244
5 T	0.00198	2.392E−7	2.521E-4	2.009E−6	1107.713	9048.631	298
J4(x=0.3, y=0.24)							
0 T	0.00265	4.740E−7	6.959E−4	9.826E−7	1399.960	20476.486	245
5 T	0.00159	2.563E−7	4.612E−4	4.954E−6	711.981	5613.429	316
J5(x=0.98, y=0.8)							
0 T	0.00231	4.832E−7	4.640E−4	1.253E−6	1415.758	23347.058	243
5 T	0.0017	2.863E−7	3.141E−4	2.283E−6	1165.636	9968.548	286

of the parameters (ρ_0, ρ_2, $\rho_{4.5}$, ρ_α, and E_a) vary systematically with varying the *A*-site disorder σ^2. It can be seen that the results calculated from Eq. (7) agree well with the experimental data. The percolation approach assumes that the materials are composed of PM and FM regions. The insulator-like transport properties are exhibited in the paramagnetic regions, while metallic transports always show up in FM regions. Then the electrical resistivity of the system at any temperature is determined by the change of the FM volume fractions in both regions.

The temperature dependence of the volume concentration of the FM phase f derived from approximation data of the experimental ρ (T) results under zero and magnetic field is shown in Fig. 4. When temperature is considerably below T_C, the f is close to 1. But when temperature increases at $T=T_C$ the concentration of the FM phase approaches zero, the transition to metallic state near T_C originates from a substantial increase in volume fraction of FMM domains on cooling towards T_C, however, the present assumption is closer to the actual situation in which both FMM domains and PMI regions randomly filled the space of the sample. The system undergoes a transition from a FM state with few PM domains at low temperature to a PM state with few FM domains at high temperature, showing the mixed-phase characteristics when the FM to PM transition occurs. This difference is caused clearly by the fact that both FMM domains and PMI regions were simply assumed to be electrically connected [32]. The present results also further verify that phase separation plays a crucial role in the transport process and the size of coexisting phase may be related to the size of the crystal grains.

As a result, T_C^{mod} is close to the T_{MI}. These results agree with the result report of Li et al. [32]. In addition, T_C^{mod} increases with magnetic field. Moreover, it can be seen for all the samples that the activation energy E_a decreases when increasing the applied magnetics field. Thus, due to the spins' attempt to align along the magnetic field, which favors the

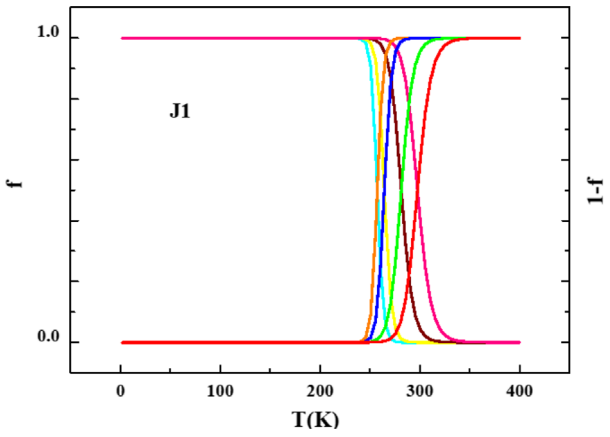

Fig. 4. The temperature dependence of ferromagnetic phase volume fraction and the paramagnetic one for ***J1*** sample.

conduction and decreases the ability of charge localization and the electrons jumping requires less energy. So the results of E_a are reasonable. The parameters ΔU may be viewed as an energy gap of the quasi-particles in the phase-separated FM and PM states.

Since magnetism is correlated with metallicity in the case of manganites, a metallic short is created due to which a metal-insulator transition takes place at $T_C < T < T_G$. In this context, the temperature derivative of the volume fraction f obtained by fitting the data to the percolation model is plotted in Fig. 5 along with the temperature dependence of the inverse of susceptibility. It is evident that the onsets of metallicity does not coincide with T_C but occurs at $T_C < T < T_G$. Different theoretical models suggest that both MI transition and GP are due to the percolative nature of electrical conduction [9,33]. In fact, among the effects that characterizes GP: the ferromagnetic metallic clusters start to interact with each other leading

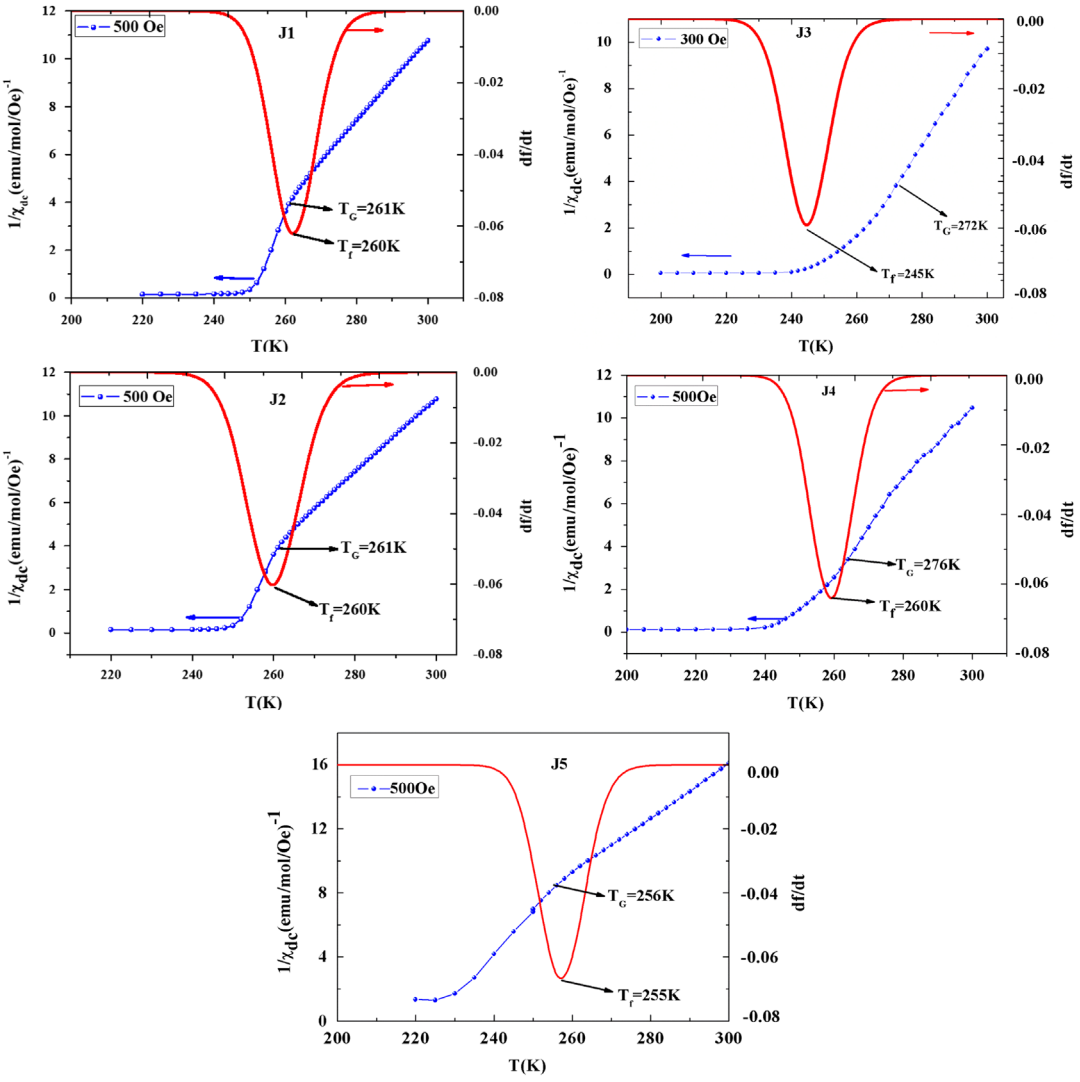

Fig. 5. Temperature dependence of the inverse of susceptibility (symbols) and the temperature derivative of metallic volume fraction f (solid lines). Upward arrow points to T_C and the downward arrow to T_G.

to a metallic-short path. This behavior leads to a metal–insulator transition even before the bulk of the material becomes fully ferromagnetic which occurs only at T_C. On the other hand, the mechanism of DE magnetic predicts that clusters are metal due to the ferromagnetic order of the Mn spins. For all the samples we can used Griffiths theory with incorporating DE mechanism, due to the fact that T_f and T_{MI} are very close to T_G.This phenomena can be explained by the decrease in the distance between the FMM clusters in the region $T_C < T < T_G$ which formed by randomly distributed PMI clusters. As consequence this FMM clusters can be easily interact between then leading a MI transition at $T \approx T_G$.

3.3. Magnetoresistance behavior

The magnetoresistance MR is defined as $\%MR = 100 \times [(\rho(0,T) - \rho(H,T))/\rho(0,T)]$ where $\rho(0,T)$and $\rho(H,T)$are the resistivity at temperature without magnetic field and in the applied magnetic field H, respectively. It is well known that the MR in manganite samples is due to the intrinsic component that arises due to the FM-DE and peaks around T_C/T_{MI} [34]. Fig. 6 shows the temperature dependent of the %MR values under applied fields 3T and 5T of the $(La_{1-x}Nd_x)_{2/3}(Ca_{1-y}Sr_y)_{1/3}MnO_3$ samples. The maximum of the %MR increase with increasing disorder σ^2 and no anomalies detected for all the samples.

It is noteworthy that the effect of disorder is slightly influence the resistivity and the %MR of $(La_{1-x}Nd_x)_{2/3}(Ca_{1-y}Sr_y)_{1/3}MnO_3$. Indeed, Akahoshi et al. [35] are the first noted that without a certain amount of disorder the CMR effect is absent. The theoretical prediction of Sen et al. [36] and Salafranca et al. [37] stating that the disorder in manganites can promote MI transition. In other several reports, it is argued that the CMR effect should be treated in the context of a Griffith's singularity driven by intrinsic randomness, the combined effect of doping, the tendency for charge segregation and the self-trapping effect associated with polaron formation [9,38]. Tong et al. [39] indicated that the GP is not necessary to be tied with the CMR in the electron doped manganites. They indicated that the strain field, in addition to quenched disorders, may be an alternative approach to understand the

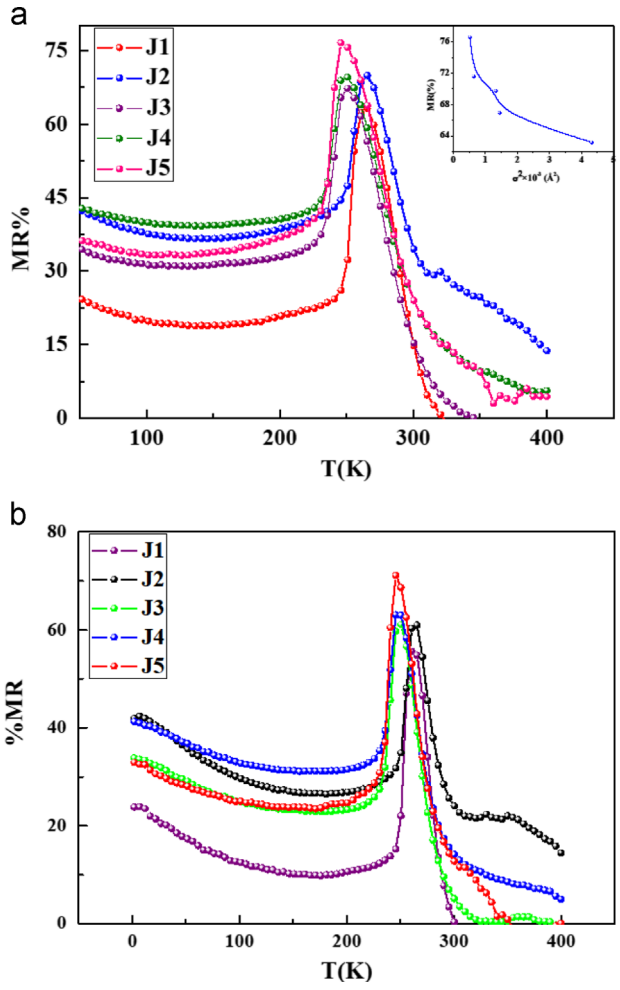

Fig. 6. The variation of %MR with temperature for $(La_{1-x}Nd_x)_{2/3}(Ca_{1-y}Sr_y)_{1/3}MnO_3$ samples under (a) $H=5$ T and (b) $H=3$ T.

observed GP. Jiang et al. [21] also reported that the GP account for CMR is not a prerequisite in manganite.

Further, in $(La_{1-x}Nd_x)_{2/3}(Ca_{1-y}Sr_y)_{1/3}MnO_3$ compounds, the increasing of %MR with disorder is explained by the presence of Griffiths singularity in all the samples as other previously studied. As seen clearly, for all samples that the increasing of %MR is due to the effect of doping of the Nd ionic which interrupts the connection of long-range Mn chains and introduces the magnetic disorder into the system which causes an enhancement of the %MR as compared with the DE of Mn^{3+}–Mn^{4+} in compound ***J1***. Such enhancement of the room temperature magnetoresistance is correlated with the shifts of the Curie temperature to near room temperature induced by the appropriate Nd doping which clearly seen in the work of Hongwei Qin et al. [40].

4. Conclusion

In conclusion, the influence of quenched disorder on the magnetic and transport properties of $(La_{1-x}Nd_x)_{2/3}(Ca_{1-y}Sr_y)_{1/3}MnO_3$ polycrystalline samples is analyzed within the context of percolative transport and the existence of the GP. The temperature dependence of magnetic susceptibility at higher temperature reveals the presence of the GP for all the samples. The transition temperatures T_{MI} characterized the electrical behavior depend on the A-site cation radii distribution function, σ^2.The conduction mechanism was explained by a small polaron hopping in the insulating region, and by electron scattering mechanisms in the metallic region. To understand the transport mechanism in the entire temperature range, we have used the phenomenological percolation model, which is based on the phase segregation of ferromagnetic metallic clusters and paramagnetic insulating regions. Also we demonstrate that magnetoresistance increase with disorder σ^2.

Acknowledgments

This work is supported by the Tunisian National Ministry of Higher Education, Scientific Research and the French Ministry of Higher Education and Research of CMCU 10G1117 collaboration, within the frame work of collaboration Franco-Tunisian.

References

[1] J.M.D. Coey, M. Viret, S. von Molnar, Advances in Physics 48 (1999) 167.
[2] P.K. Siwach, H.K. Singh, O. Srivastava, Journal of Physics: Condensed Matter 20 (2008) 273201.
[3] M. Md, L. Seikh, C.N.R. Sudheendra, Rao, Journal of Solid State Chemistry 177 (2004) 3633.
[4] S. Othmani, M. Bejar, E. Dhahri, E.K. Hlil, Journal of Alloys and Compounds 475 (2009) 46.
[5] S. Othmani, R. Blel, M. Bejar, M. Sajieddine, E. Dhahri, E.K. Hlil, Solid State Communications 149 (2009) 969.
[6] C. Zener, Physical Review 82 (1951) 403;
PW. Anderson, H. Hasegawa, Physical Review 100 (1955) 675.
[7] J.A. Millis, BP. Littlewood, IB. Shraiman, Physical Review Letters 74 (1995) 5144.
[8] E. Dagotto, Nanoscale Phase Separation and Colossal Magnetoresistance, Springer, Berlin, 2002.
[9] M.B. Salamon, P. Lin, SH. Chun, Physical Review Letters 88 (2002) 197203.
[10] J. Burgy, M. Mayr, V. Martin-Mayor, A. Moreo, E. Dagotto, Physical Review Letters 87 (2001) 277202.
[11] R.B. Griffiths, Physical Review Letters 23 (1969) 17.
[12] P. Tong, et al., Physical Review B 77 (2008) 184432.
[13] J. Khelifi, Journal of Superconductivity and Novel Magnetism, http://dx.doi.org/10.1007/s10948-013-2131-6, in press.
[14] J.M. De Teresa, M.R. Ibarra, P.A. Algarabel, C. Ritter, C. Marquina, J. Balasco, J. Garcia, A. del. Moral, Z. Arnold, Nature 386 (1997) 256.
[15] S. Cao, B. Kang, J. Zhang, S. Yuan, Applied Physics Letters 88 (2006) 172503.
[16] N. Volkov, G. Petrakovskii, K. Patrin, K. Sablina, E. Eremin, V. Vasiliev, M. Molokeev, P. Boni, E. Clementyev, Physical Review B 73 (2006) 104401.
[17] W.J. Lu, Y.P. Sun, W.H Song, J. Du, Journal Solid State Communications 138 (2006) 200.
[18] Y. Imry, S-K. Ma, Physical Review Letters 35 (1975) 1399.
[19] A. Moreo, M. Mayr, A. Feiguin, S. Yunoki, E. Dagotto, Physical Review Letters 84 (2000) 5568.
[20] H. Yi, N.H. Hur, J. Yu, Physical Review B 61 (2000) 9501.
[21] W. Jiang, X.Z. Zhou, G. Williams, Y. Mukovskii, K. Glazyrin, Physical Review Letters 99 (2007) 177203;
W. Jiang, X.Z. Zhou, G. Williams, Y. Mukovskii, K. Glazyrin, Physical Review B 76 (2007) 092404;
W. Jiang, X.Z. Zhou, G. Williams, Y. Mukovskii, K. Glazyrin, Physical Review B 77 (2008) 064424.

[22] G. Bouzerar, O. Ce´pas, Physical Review B 76 (R) (2007) 020401.
[23] J.W. Chen, G. Narsinga Rao, Materials Chemistry and Physics 136 (2012) 254–258.
[24] E. Rozenberg, M. Auslender, A.I. Shames, G. Gorodetsky, Ya. M Mukovskii, Applied Physics Letters 92 (2008) 2222506;
M. Auslender, A.I. Shames, E. Rozenberg, G. Gorodetsky, Ya. M. Mukovskii, Journal of Applied Physics 105 (2009) 07D705.
[25] T.J. Sato, J.W. Lynn, B. Dabrowski, Physical Review Letters 93 (2004) 267204.
[26] G. Venkataiah, V. Prasad, P.Venugopal Reddy, Solid State Communications 141 (2007) 73.
[27] L.M. Rodriguez-Martinez, J.P. Attfield, Physical Review B 54 (1996) R15622.
[28] G Li, H-D Zhou, S.L Feng, X-J Fan, X.G Li, Journal of Applied Physics 92 (2002) 1406.
[29] N. Panwar, V. Sen, D.K. Pandya, S.K. Agarwal, Materials Letters 61 (2007) 4879.
[30] I.K. Kamilov, A.G. Gamzatov, A.M. Aliev, A.B. Batdalov, S. B. Abdulvagidov, O.V. Melnikov, O.Y. Gorbenko, A.R. Kaul, Kinetic effects in manganites $La_{1-x}Ag_yMnO_3$ $(y-x)$, Journal of Experimental and Theoretical Physics 105 (2007) 774.
[31] S.B. Abdulvagidov, A.G. Gamzatov, O.V. Melnikov, O. Yu., Gorbenko, Influence of the lanthanum deficit on electrical resistivity and heat capacity of silver-doped lanthanum manganites $La_{1-x}Ag_yMnO_3$, Journal of Experimental and Theoretical Physics 109 (2009) 989.
[32] S.L. Yuan, W.Y. Zhao, G.Q. Zhang, F. Tu, G. Peng, J. Liu, Y.P. Yang, G Li, Y. Jiang, X.Y. Zeng, C.Q. Tang, S.Z. Jin, Applied Physics Letters 77 (2000) 4398;
S.L. Yuan, Z.Y. Li, W.Y. Zhao, G. Li, X.Y. Zeng, Y.P. Yang, G. Q. Zhang, F. Tu, C.Q. Tang, S.Z. Jin, Physical Review B 63 (2001) 172415.
[33] V.N. Krivoruchko, M.A. Marchenko, Y. Melikhov, Physical Review B 82 (2010) 064419.
[34] X.L. Wang, et al., Applied Physics Letters 73 (1998) 396.
[35] D. Akahoshi, M. Uchida, Y. Tomioka, T. Arima, Y. Matsui, Y. Tokura, Physical Review Letters 90 (2003) 177203.
[36] C. Sen, G. Alvarez, E. Dagotto, Physical Review B 70 (2004) 064428.
[37] J. Salafranca, L. Brey, Physical Review B 73 (2006) 214404.
[38] J. Burgy, M. Mayr, V. Martin-Mayor, A. Moreo, E. Dagotto, Physical Review Letters 87 (2001) 277202.
[39] P. Tong, B. Kim, D. Kwon, T. Qian, Lee Sung-IK, S-W Cheong, B. G. Kim, Physical Review B 77 (2008) 184432.
[40] Qin. Hongwei, Hu. Jifan, Chen. Juan, Zhu. Luming, Niu. Hongdong, Materials Transactions 45 (2004) 1251–1254.